

Full Motion Compensation for LFM-CW Synthetic Aperture Radar

Evan C. Zaugg and David G. Long

Brigham Young University Microwave Earth Remote Sensing Laboratory
459 Clyde Building, Provo, UT 84602 801-422-4884 zaugg@mers.byu.edu

Abstract—Small, low-cost, high-resolution SAR systems, such as the Brigham Young University (BYU) μ SAR, are made possible by using a linear frequency modulated continuous wave (LFM-CW) signal. SAR processing assumes that the sensor is moving in a straight line at a constant speed, but in actuality a UAV or airplane will deviate, often significantly, from this ideal. This non-ideal motion can seriously degrade the SAR image quality. In a continuous wave system this motion happens during the radar pulse which means that existing motion compensation techniques, which approximate the position as constant over a pulse, are limited for an LFM-CW SAR. In this paper, the LFM-CW SAR signal model is presented and processing algorithms are discussed. The effects of non-ideal motion during the SAR signal are derived and new methods for motion correction are developed which correct for motion during the pulse. These new motion correction algorithms are verified with simulated data and with actual data collected using the BYU μ SAR system.

I. INTRODUCTION

Recently very small low-cost SAR systems have been demonstrated as an alternative to the expensive and complex traditional systems. The successful operation of the BYU μ SAR has shown the viability of such a SAR [1]. The use of an LFM-CW signal facilitates system miniaturization and low-power operation which make it possible to fly the μ SAR on a small UAV. The ease of operation and low operating costs make it possible to conduct extensive SAR studies without a large investment.

The BYU μ SARs are small, student-built, low-power, LFM-CW SAR systems. They weigh less than 2 kg, including antennas and cabling, and consume 18 watts of power. The μ SAR systems operate at C-band or L-band with bandwidths of 80-160 MHz. Units have been successfully flown in the arctic and extensively operated over Utah and Idaho.

Basic stripmap SAR processing assumes that the platform is moving in a straight line, at a constant speed, and with a consistent geometry with the target area. During data collection, whether in a manned aircraft or a UAV, there are deviations from this ideal as the platform changes its attitude, speed, or is subjected to turbulence in the atmosphere. These displacements introduce variations in the phase history, the signal's time of flight to a target, and the sample spacing, all of which degrade the image quality. If the motion of the platform is known, then corrections can be made to the SAR data for more ideal image processing.

Motion compensation algorithms for traditional pulsed SAR have been extensively studied, but the underlying differences with an LFM-CW signal make it a challenge to extend existing

motion compensation methods to LFM-CW sensors. In pulsed SAR, the platform is often assumed to be stationary during each pulse and the motion takes place between pulses. With a LFM-CW SAR the signal is constantly being transmitted and received, thus the motion takes place during the chirp.

This paper presents the development of new motion compensation algorithms that account for the motion during the chirp. First, the theoretical underpinnings of LFM-CW SAR and the effect of non-ideal motion are used to develop correction algorithms. Next, simulator results are shown where a SAR system moves past a few point targets with non-ideal motion. The deviations are used to compensate for the effects of non-ideal motion in the simulated data.

The developed algorithms are then applied to actual μ SAR data at both C- and L-bands and the results are presented. Motion data is provided by an inertial navigation system and GPS. The flight path data is interpolated between samples to provide position data for each sample of SAR data. The motion data is used to determine the necessary corrections which are introduced into the SAR data, effectively straightening the flight path.

II. LFM-CW SAR SIGNAL PROCESSING

In a symmetric LFM-CW chirp the frequency of the signal increases from a starting frequency ω_0 , and spans the bandwidth BW , at the chirp rate $k_r = BW \cdot 2 \cdot PRF$. The frequency then ramps back down as seen in Fig. 1 This up-down cycle is repeated at the PRF, giving a PRI of T_p . The transmitted up-chirp signal can be expressed in the time domain, where t is fast-time and η is slow time, as

$$s_t(t, \eta) = e^{j(\phi + \omega_0 t + \pi k_r t^2)}, \quad (1)$$

where ϕ is the initial phase. The down chirp is similar with $\omega_0 + BW$ being the starting frequency and $-k_r$ the chirp rate.

The received signal from a target at range $R(t, \eta) = \sqrt{R_0^2 + v^2(t + \eta)^2}$, with time delay $\tau = 2R(t, \eta)/c$ is

$$s_r(t, \eta) = e^{j(\phi + \omega_0(t - \tau) + \pi k_r(t - \tau)^2)}. \quad (2)$$

The transmit signal is mixed with the received signal and low-pass filtered in hardware, which is mathematically equivalent to multiplying Eq. (1) by the complex conjugate of Eq. (2). This results in the de-chirped signal

$$s_{dc}(t, \eta) = e^{j(\omega_0 \tau + 2\pi k_r t \tau - \pi k_r \tau^2)}. \quad (3)$$

For Range-Doppler Algorithm (RDA) processing, this signal is range compressed with an FFT in the range direction then

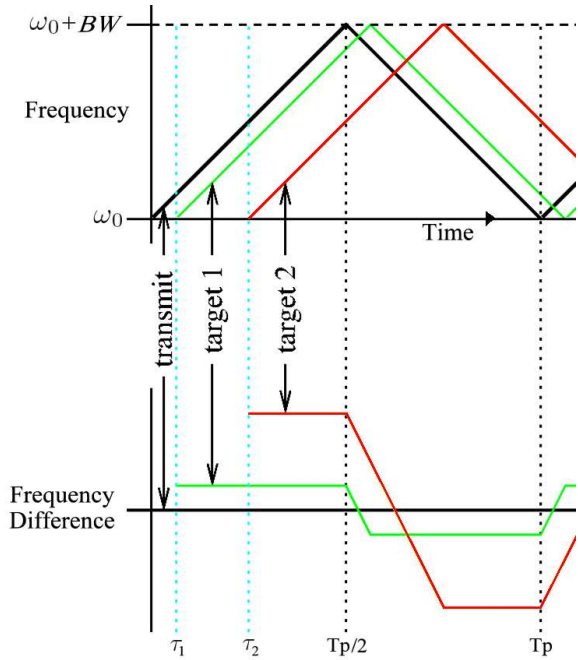


Fig. 1. The frequency change of a symmetric LFM-CW signal over time is shown above together with the signal returns from two separate targets. The frequencies of the de-chirped signal are shown below, with the times of flight, τ_1 and τ_2 , due to range determining the de-chirped frequency. The relative sizes of τ_1 , τ_2 , and T_p are exaggerated for illustrative purposes.

taken to the range-Doppler domain with an FFT in the azimuth direction. Using standard interpolation methods the range cell migration (RCM) can be compensated and the Doppler shift introduced by the continuous motion of the platform can be removed [2]. The azimuth compression is performed by multiplying by the azimuth matched filter

$$H_{az}(f_\eta, R_0) = e^{j2\omega_0 R_0 D(f_\eta, v)/c}, \quad (4)$$

where $D(f_\eta, v) = \sqrt{1 - \lambda^2 f_\eta^2 / 4v^2}$ is the range migration

factor and v is the platform along-track velocity.

Alternatively, the Frequency (or Chirp) Scaling Algorithm (FSA or CSA) [3] can also be modified to work with the de-chirped data [4]. With the FSA, the RCM and Doppler shift can be compensated without interpolation [5]. A Fourier transform is performed in the azimuth direction on the signal from Eq. (3). The resulting signal in the de-chirped-Doppler domain is

$$S(t, f_\eta) = e^{-j\frac{4\pi R_0 D(f_\eta, v)}{\lambda}} e^{-j\frac{4\pi k_r R_0 t}{cD(f_\eta, v)}} e^{j2\pi f_\eta t} e^{-j\pi k_r t^2}. \quad (5)$$

A filter is applied which removes the Doppler shift and scales the frequency,

$$H_1(t, f_\eta) = e^{-j(2\pi f_\eta t + \pi k_r t^2 (1 - D(f_\eta, v)))}. \quad (6)$$

A range FFT is performed and the second filter is applied which corrects the residual video phase,

$$H_2(f_r, f_\eta) = e^{(-j\pi f_r^2)/(k_r D(f_\eta, v))}. \quad (7)$$

An inverse FFT in the range direction is performed followed by a filter that performs an inverse frequency scaling,

$$H_3(t, f_\eta) = e^{-j\pi k_r t^2 [D(f_\eta, v)^2 - D(f_\eta, v)]}. \quad (8)$$

We again take the range FFT and apply the final filter that performs the azimuth compression,

$$H_4(R, f_\eta) = e^{j\frac{4\pi R}{\lambda} D(f_\eta, v)}. \quad (9)$$

An azimuth IFFT results in the final focused image.

III. NON-IDEAL MOTION ERRORS

The SAR processing algorithms described in section II assume that the platform moves at a constant speed in a straight line. In any actual data collection this is not the case, as the platform experiences a variety of deviations from the ideal path. These deviations introduce errors in the collected data which cause degradation of the SAR image.

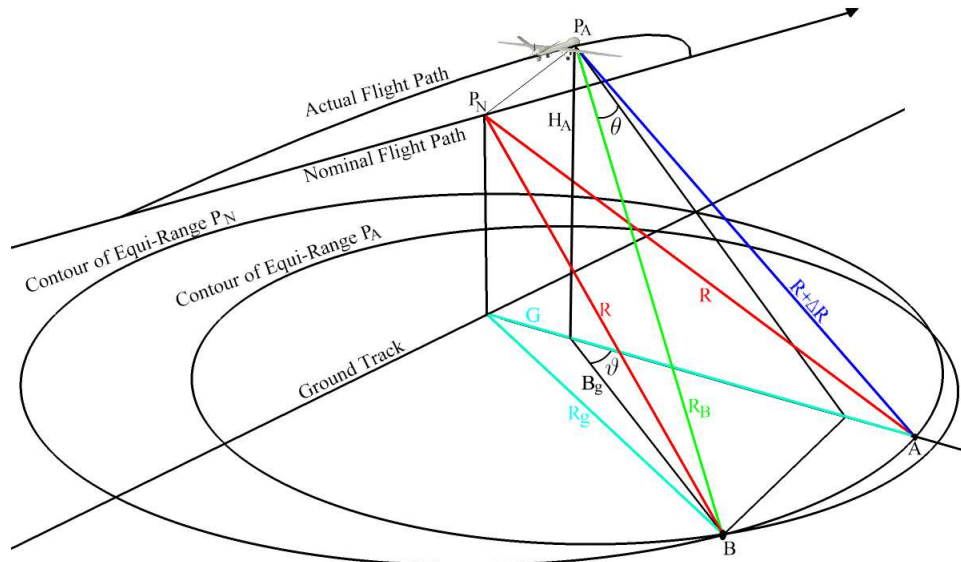


Fig. 2. The SAR platform deviates from its nominal path, point P_N , resulting in a change in range to point A from R to $R + \Delta R$. Point B is nominally at a range R , but the deviation to point P_A changes the range to R_B , which is different from ΔR .

Translational motion causes platform displacement from the nominal, ideal path, this results in the target scene changing in range during data collection. A target at range R is measured at range $R + \Delta R$ resulting in a frequency shift in the de-chirped data. The de-chirped signal in Eq. (3) then becomes

$$s_{\Delta dc}(t, \eta) = e^{-\frac{1}{2}j(\tau + \Delta\tau)(2\pi k_r \Delta\tau - 2\omega_0 - 4\pi k_r t + 2\pi k_r \tau)}. \quad (10)$$

where $\Delta\tau = 2\Delta R/c$. Targets that lie within the beamwidth that have a non-zero Doppler frequency experience a different change in range dependent on the azimuth position. This is illustrated in Fig. 2 where the range to target A changes with motion differently than the range to target B .

Variations in along-track ground speed result in non-uniform spacing of the radar pulses on the ground. This non-uniform sampling of the Doppler spectrum results in erroneous calculations of the Doppler phase history.

Changes in pitch, roll, and yaw introduce errors of a different kind. The pitching displaces the antenna footprint on the ground, the roll changes the antenna gain pattern over the target area, and the yaw introduces a squint. Pitch and yaw shift the Doppler centroid, with the shift being range dependent in the yaw case. If the Doppler spectrum is shifted so that a portion lies outside the Doppler bandwidth, then aliasing occurs. The azimuth compression produces ghost images at the azimuth locations where the Doppler frequency is aliased to zero.

IV. MOTION COMPENSATION

Previously developed methods of motion compensation are limited for correcting the non-ideal motion of an LFM-CW SAR system. Methods like those of [6] apply a bulk motion compensation to the raw data and a secondary correction to the range compressed data. This works as an approximation for motion correction, but relies on assuming the platform is stationary during a pulse. In range compressing the data, we lose the ability to differentiate the motion over the chirp, which is problematic for LFM-CW SAR.

For an LFM-CW SAR signal, the motion corrections can be applied directly to the raw de-chirped data (Eq. 10). Doppler dependent corrections are applied to the azimuth FFT of the raw data, in the de-chirped-Doppler domain. Because each data point contains information from every range, and the corrections are range and azimuth dependent, any corrections applied in the de-chirped-Doppler domain are valid for only one single range and one azimuth value. However, with approximations these restrictions can be relaxed.

A. Range Cell Migration Correction

While not a result of non-ideal motion, the RCM can be corrected without interpolation for the RDA using techniques which demonstrate the methods used for motion compensation. With the data in the de-chirped-Doppler domain, the RCM is calculated for a given range R_0 and Doppler frequency f_η

$$R_{RCM}(R_0, F_\eta, v) = R_0/D(f_\eta, v). \quad (11)$$

This range differs from our target range by $\Delta R = R_0 - R_{RCM}$ giving $\Delta\tau = 2\Delta R/c$. We apply the correction by multiplying

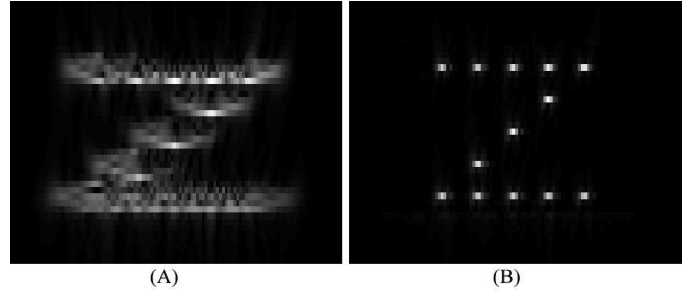


Fig. 3. Simulated LFM-CW SAR data of an array of 13 point targets with non-ideal motion (sinusoidal translational). The data is processed without motion compensation in (A) resulting in azimuth and range smearing of the targets. The same data is processed again using the motion compensation algorithms developed in this paper with the results shown in (B).

the data in the de-chirped Doppler domain by our correction filter

$$H_{MC}(t, \Delta\tau) = e^{\frac{1}{2}j\Delta\tau(4\pi k_r \tau + 2\pi k_r \Delta\tau - 4\pi k_r t - 4\pi k_r \tau)}. \quad (12)$$

When correcting the RCM for use with the RDA, after applying the correction for a given range, R_0 , an IFFT takes the data back into the time domain, an FFT performs range compression and the data in range bin R_0 is saved. The process is repeated for each value of R_0 , and the composite of the corrected range bins is azimuth compressed for the final image.

B. Translational Motion Correction

In general, motion data is collected at a much slower rate than SAR data. For LFM-CW SAR the motion data must be interpolated so that every sample of SAR data has corresponding position information (as opposed to only each pulse having position data). Each data point also needs to have a corresponding location on the ideal path to which the error is corrected.

If the beamwidth is narrow then the errors due to motion can be assumed to be constant for a given range across the Doppler bandwidth. This simplifies the analysis. The flat-terrain geometry of Fig. 2 is assumed. If more precise knowledge of the terrain is available then the model can be adjusted. Knowing the coordinates of target A , the actual flight path (point P_A), and the nominal flight path (point P_N), the distances R and $R + \Delta R$ can be calculated from geometry. Again $\Delta\tau = 2\Delta R/c$, but $\Delta\tau$ is updated for every data sample. Since we are assuming no Doppler dependence on the correction, we can apply Eq (12) directly to the raw de-chirped data. Once the corrections for a given range have been applied, processing continues using either RDA or CSA until range compression is completed. As with the RCM correction formulated earlier, the correction is valid for only a single range, thus a composite range compressed image is created and then azimuth compressed to form the final image.

If the beamwidth is wide, then there are targets at the same range but different azimuth positions that experience a different range shift due to translational motion. For a given azimuth position, see Fig. 2, target B is at a position where it has the Doppler frequency f_η . The angle to target B is

$$\theta(f_\eta) = \sin^{-1} \left(\frac{f_\eta \lambda}{2v} \right). \quad (13)$$

Working through some particularly unpleasant geometry, the angle on the ground (as defined in Fig. 2) $\vartheta(\theta(f_\eta), R_g, G, H_A)$ is found. From ϑ we find the ground range,

$$B_g(f_\eta) = -\cos(\vartheta)G \pm \sqrt{\cos^2(\vartheta)G^2 + R_g^2 - G^2}, \quad (14)$$

and the actual range to target B ,

$$R_B(f_\eta) = \sqrt{H_A^2 + B_g^2}. \quad (15)$$

We then find $\Delta R = R - R_B(f_\eta)$, $\Delta\tau = 2\Delta R(f_\eta)/c$, and apply Eq. (12) in the de-chirped-Doppler domain. This correction is valid for a single range and azimuth position and can be combined with RCM correction in a single step.

C. Velocity and Attitude

Platform velocity can also vary with time. Traditionally the data is interpolated in the azimuth direction to correct for the velocity variations across the synthetic aperture. Alternatively, the filters used in processing can be modified to match the changes in velocity.

Attitude errors generally produce negligible amounts of range displacement and principally affect the gain of the SAR image. Gain variations can usually be handled by rescaling the complex SAR image.

D. Minimizing Doppler Aliasing

Doppler aliasing occurs when the platform velocity exceeds the allowable range for a given PRF or when the pitch or yaw of the platform shifts the illuminated ground swath such that the return signal contains Doppler frequencies outside the Doppler bandwidth. A symmetric LFM-CW signal offers a unique opportunity to minimize aliasing by exploiting the fact that for each pulse cycle there is both an up-chirp and a down-chirp which can be treated individually as successive pulses, effectively doubling the PRF. The signal for the up-chirp is given by Eqn. (1) with the recorded de-chirped signal given in Eqn. (3). The down chirp is

$$s_t(t, \eta) = e^{j(\phi + (\omega_0 + \frac{k_r T_p}{2})(t + \frac{T_p}{2}) - \pi k_r (t + \frac{T_p}{2})^2)}, \quad (16)$$

with the corresponding de-chirped signal

$$s_{dc}(t, \eta) = e^{-\frac{T_p}{2} j\tau(\frac{-2\omega_0}{T_p} - \beta + \frac{4\pi\beta t}{T_p} + 2\pi\beta - \frac{2\pi\beta\tau}{T_p})}. \quad (17)$$

This can be made to match the up-chirp by multiplying Eqn. (17) by

$$h_{du} = e^{\frac{T_p}{2} j\tau(\frac{-4\pi\beta\tau}{T_p} + \frac{4\beta t}{T_p} - \beta + 2\pi\beta)}. \quad (18)$$

V. MOTION COMPENSATION RESULTS: SIMULATION AND μ SAR DATA

An LFM-CW SAR signal from an array of point targets is simulated. Non-ideal motion is introduced into the motion of the platform, including changes in velocity, platform displacement, and attitude changes. The known deviations are successfully used to correct the effects of the non-ideal motion. An example can be seen in Fig. 3.

The BYU μ SAR is flown with an INS/GPS unit which measures the motion of the airplane. As discussed, the motion data is interpolated and matched with the actual SAR data. The results are seen in Fig. 4 where the motion corrections are shown to improve the image.

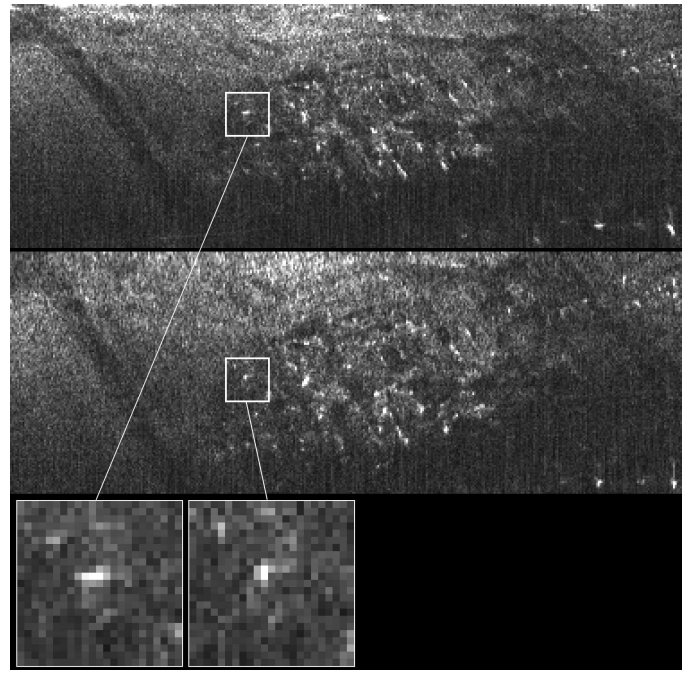


Fig. 4. The town of Newton, Utah imaged with a 160 MHz bandwidth μ SAR. The top image is without motion compensation, the middle shows the motion corrected image, and the lower images are expanded views of a point target. The motion correction improves the focusing of point targets and straightens the roads (visible on the left and right sides) that were artificially curved by non-ideal motion of the airplane. This multilook image has a resolution of about 1 meter per pixel. Image quality is degraded by Doppler aliasing.

VI. CONCLUSION

In this paper the effects of non-ideal motion on an LFM-CW SAR signal have been explored and corrective algorithms developed. The motion compensation has been successfully applied to simulated and real SAR data. The small size of the BYU μ SAR makes it possible for it to operate from a small aircraft or UAV, which may be especially susceptible to the effects of atmospheric turbulence. With motion measurements, the negative effects of non-ideal motion can be corrected, extending the utility of small LFM-CW SAR.

REFERENCES

- [1] E.C. Zaugg, D.L. Hudson, and D.G. Long, "The BYU μ SAR: A Small, Student-Built SAR for UAV Operation", in *Proc. Int. Geosci. Rem. Sen. Symp.*, Denver Colorado, pp.411-414, Aug. 2006.
- [2] J.J.M. de Wit, A. Meta, and P. Hooeboom, "Modified range-Doppler processing for FM-CW synthetic aperture radar", in *IEEE Geoscience and Remote Sensing Letters*, vol. 3, pp. 83-87, Jan. 2006.
- [3] I.G. Cumming and F.H. Wong, *Digital Processing of Synthetic Aperture Radar Data*, Artech House, 2005.
- [4] J. Mittermayer, A. Moreira, and O. Loffeld, "Spotlight SAR data processing using the frequency scaling algorithm", in *IEEE Trans. Geosci. Remote Sensing*, vol. 37, pp. 2198-2214, Sept. 1999.
- [5] A. Meta, P. Hooeboom, and L.P. Ligthart, "Non-linear Frequency Scaling Algorithm for FMCW SAR Data", in *Proc. 3rd European Radar Conference, 2006*, pp. 9-12, Sept. 2006.
- [6] A. Moreira, and Y. Huang, "Airborne SAR processing of highly squinted data using a chirp scaling approach with integrated motion compensation", in *IEEE Trans. Geosci. Remote Sensing*, vol. 32, pp. 1029-1040, Sept. 1994.